AIAA JOURNAL
Vol. 34, No. 11, November 1996

Spatial Evolution of a Monochromatically Forced Flat-Plate Wake

D. I. Dratler* and H. F. Fasel†
University of Arizona, Tucson, Arizona 85721

Nonlinear disturbance development in a two-dimensional, incompressible, spatially developing wake behind a thin flat plate aligned parallel to a uniform freestream is investigated by direct numerical integration of the Navier–Stokes equations. For the numerical integration, finite difference methods together with an alternating direction implicit/Adams–Bashforth time integration scheme are employed. The wake is harmonically forced at the inflow boundary at the frequency of maximum amplification predicted by linear stability theory. The response to this monochromatic forcing includes a disturbance component at the forcing frequency that grows very rapidly before saturating a short distance downstream. This saturation can be predicted qualitatively from a linear stability analysis of the distorted mean flow. Farther downstream, the disturbance energy is concentrated in the fundamental disturbance, the second harmonic, and the mean-flow distortion component. At large amplitudes, a Kármán vortex street forms. Variations in forcing strength do not alter the qualitative behavior of the forced wake. The results of these simulations compare well with both linear stability theory and experimental measurements.

Nomenclature

A = parameter that characterizes the forcing strength
b = wake half-width, defined as the cross-stream location at which u is halfway between the freestream and the centerline velocities
E_l = disturbance kinetic energy associated with temporal mode l
$\bar{L}$ = length of wake-generating flat plate
l = frequency mode number
M = number of grid points in the cross-stream direction
N = number of grid points in the streamwise direction
Re = Reynolds number, $\bar{U}_\infty \bar{L}/\bar{\nu}$
r = $\bar{\theta}_{TE}/\bar{L}$
s = ramp function
t = time
U_c = wake centerline velocity
$\hat{U}_l$ = amplitude of time-periodic streamwise perturbation velocity
$\bar{U}_\infty$ = freestream velocity
u = streamwise velocity
u_i = undisturbed streamwise velocity at the inflow boundary
$\hat{u}(y)$ = amplitude of streamwise component of the Orr–Sommerfeld eigenfunction corresponding to the frequency β
u' = streamwise perturbation velocity
$\hat{V}_l$ = amplitude of time-periodic cross-stream perturbation velocity
v = cross-stream velocity
x = streamwise distance
x_i = streamwise location of inflow boundary
x_o = streamwise location of outflow boundary
y = cross-stream distance
y_l = cross-stream location of lower freestream boundary
y_u = cross-stream location of upper freestream boundary
α_i = amplification rate of fundamental disturbance
α_r = wave number of fundamental disturbance
β = frequency of Orr–Sommerfeld mode used to excite the wake
$\bar{\theta}_{TE}$ = wake momentum thickness at trailing edge of the flat plate
λ = wavelength of fundamental disturbance
$\bar{\nu}$ = kinematic viscosity
$\hat{\phi}_u(y)$ = phase of streamwise component of Orr–Sommerfeld eigenfunction corresponding to the frequency β
ω_z = spanwise vorticity

All quantities are dimensionless except those with an overbar.

I. Introduction

In spite of considerable research effort spanning many decades, laminar-turbulent transition in wake flows is still poorly understood. Much of what is known is attributable to the experimental work of Sato and Kuriki,[1] who investigated laminar-turbulent transition in wakes generated by thin flat plates. Their experiments have shown that the initial stages of laminar-turbulent transition in the low-speed regime is predominantly two dimensional. In these initial stages, which can be described by linear stability theory for only a small region near the trailing edge of the plate, disturbances rapidly attain large amplitudes. As a result, nonlinear effects become important very early in the transition process. On the basis of their measurements, Sato and Kuriki concluded that this nonlinearity leads to a reduction in disturbance growth rates, distortion of fundamental disturbance amplitude and phase distributions, generation of higher harmonics, and significant distortion of the mean flow. In particular, their results indicated a significant increase in the wake width and centerline velocity, and the appearance of velocity overshoots at the edge of the deficit region. They noted that some of these observations are consistent with the development of a staggered vortex-street pattern, i.e., a Kármán vortex street. Consistent with this conjecture, the experiments of Heinemann et al.[2] have shown that Kármán vortex streets do develop in flat-plate wakes.

In a number of more recent investigations, direct numerical simulations have been used to investigate the two-dimensional stages of wake transition. These simulations, which include the works of Zabusky and Deem,[3] Hannemann and Oertel,[4] and Maekawa et al.,[5] have confirmed many of Sato and Kuriki's[1] findings. In one of the first works of its kind, Zabusky and Deem[3] performed simulations based on the full Navier–Stokes equations to investigate the temporal evolution of wakes subjected to monochromatic initial fluctuations. Their results indicated initial exponential growth of the wake fluctuation, followed by a much longer period of nonlinear evolution that eventually led to the development of a classic Kármán

Received Oct. 11, 1995; revision received April 24, 1996; accepted for publication May 24, 1996; also published in *AIAA Journal on Disc*, Volume 1, Number 4.

*Research Associate, Department of Aerospace and Mechanical Engineering; currently Research Engineer, Exxon Production Research Company, P.O. Box 2189, Houston, TX 77252-2189. Senior Member AIAA.

†Professor, Department of Aerospace and Mechanical Engineering. Senior Member AIAA.

vortex-street pattern in the wake. Other than the assumed temporal evolution of their flow, the variation of disturbances and the mean flow were in good agreement with the measurements of Sato and Kuriki.[1] Hannemann and Oertel[4] simulated the evolution of wakes generated by a blunt-edged plate and found a significant region of absolute instability, as seen in bluff-body wakes. This absolute instability was displaced by a convective instability when the normalized centerline velocity exceeded 0.04, indicating a very small region of absolute instability in wakes behind thin plates. In the work of Maekawa et al.,[5] the effect of fundamental, subharmonic, and random forcing on wake development was investigated, with wake evolution found to be highly sensitive to the nature of excitation. However, for strictly fundamental forcing, their results were in good general agreement with the measurements of Sato and Kuriki.[1]

Despite a number of investigations of nonlinear disturbance development in wakes, including the numerical studies cited above, nonlinear processes involved in the initial stages of wake transition still are not well understood. To gain a better understanding of these processes, direct numerical simulation (DNS) has been used to investigate the initial, two-dimensional, spatial evolution of incompressible, flat-plate wakes when subjected to monochromatic forcing. Our results show that the initial deviation of fundamental disturbance growth from predictions of linear theory, including the saturation of the fundamental disturbance, can be predicted from a linear stability analysis of the distorted mean flow. This ability to describe nonlinear phenomena with a linear model is remarkable, and provides considerable insight into the mechanism leading to fundamental disturbance saturation. We then present results illustrating the effect of forcing amplitude on the disturbance development.

II. Governing Equations and Computational Domain

We consider a wake that forms downstream of a thin flat plate aligned parallel to a low-speed, uniform stream of velocity $\bar{U}_\infty$. The plate is assumed to have a length $\bar{L}$ and an infinite span. In addition, the plate trailing edge is assumed to be sharp, so that the recirculating region behind the plate is negligibly small. Under these conditions, wake instabilities are convective in nature except in a small region very close to the trailing edge of the plate (see, e.g., Huerre and Monkewitz[6]).

Simulations are performed in a computational domain located far enough downstream of the plate trailing edge to exclude the region of absolute instability, but located near enough to the plate trailing edge to include most of the high-deficit near-wake region. As shown in Fig. 1, the spatial extent of the computational domain is defined by $x_i \le x \le x_o$ and $y_l \le y \le y_u$, where x_i, x_o, y_l, and y_u have been nondimensionalized as outlined in the next paragraph. The actual physical dimensions of the computational domain are given with the discussion of the numerical results in Sec. V.

For the direct numerical simulations described in this paper, the governing equations are the incompressible Navier–Stokes equations in vorticity–velocity formulation. In two dimensions, these equations are

$$\frac{\partial \omega_z}{\partial t} + u\frac{\partial \omega_z}{\partial x} + v\frac{\partial \omega_z}{\partial y} = \frac{1}{Re}\nabla^2\omega_z \tag{1a}$$

$$\nabla^2 u = -\frac{1}{r^2}\frac{\partial \omega_z}{\partial y} \tag{1b}$$

$$\nabla^2 v = \frac{1}{r^2}\frac{\partial \omega_z}{\partial x} \tag{1c}$$

All variables in Eq. (1) are nondimensionalized according to $x = \bar{x}/\bar{L}$, $y = \bar{y}/\bar{\theta}_{TE}$, $t = \bar{t}\bar{U}_\infty/\bar{L}$, $u = \bar{u}/\bar{U}_\infty$, $v = \bar{v}/\bar{U}_\infty r$, and $\omega_z = \bar{\omega}_z\bar{\theta}_{TE}/\bar{U}_\infty$. The independent variables x and y and the parameters $\bar{\theta}_{TE}$, $\bar{L}$, and $\bar{U}_\infty$ are defined in relation to the flat plate in Fig. 1.

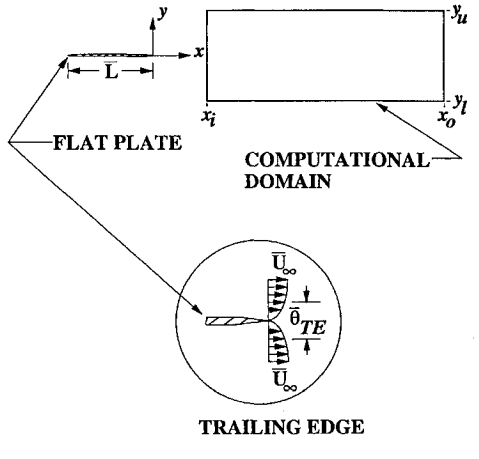

Fig. 1 Schematic of the computational domain, defined by $x_i \le x \le x_o$ and $y_l \le y \le y_u$. The inset schematically defines $\bar{U}_\infty$ and $\bar{\theta}_{TE}$.

III. Boundary and Initial Conditions

The governing equations (1) describe an initial-boundary value problem. To solve these equations, boundary conditions must be prescribed for the entire bounding surface of the computational domain, and appropriate initial conditions must be prescribed for the initial time of the calculation. In addition, the imposed boundary conditions must allow for spatial disturbance development. These conditions are now described.

A. Inflow Boundary ($x = x_i$)

At the inflow boundary, disturbances are introduced into an otherwise undisturbed wake. For this purpose, time-periodic forcing consisting of a two-dimensional Orr–Sommerfeld mode is employed. For the streamwise velocity, this boundary condition has the form

$$u(y,t) = u_i(y) + s(t)A\hat{u}(y)\cos[\alpha_r x_i - \beta t + \hat{\phi}_u(y)] \tag{2}$$

where $s(t)$ is defined by

$$s(t) = \sin^2(\beta t/2) \quad \text{for} \quad 0 \le t < \pi/\beta \tag{3a}$$

$$s(t) = 1 \quad \text{for} \quad t \ge \pi/\beta \tag{3b}$$

B. Freestream Boundaries ($y = y_l, y_u$)

At the freestream boundaries, exponential decay of the velocity fluctuations is enforced by a set of computational boundary conditions[7] of the form

$$\frac{\partial u'}{\partial y} = \pm r\alpha_r u' \tag{4}$$

In Eq. (4), the minus sign applies at $y = y_u$ and the plus sign applies at $y = y_l$. The continuity equation is used as a boundary condition for the cross-stream velocity. Vorticity disturbances typically decay very rapidly at large $|y|$; therefore, the disturbance velocity field is assumed to be irrotational at the freestream boundaries of the computational domain.

To use Eq. (4) for our simulations, which is strictly valid for small-amplitude, neutrally stable disturbances only, we adhere to at least one of the following restrictions: First, we can restrict β so that the resulting small-amplitude disturbance growth rates are low enough for Eq. (4) to be a reasonable approximation. As will be shown in Sec. V.A, Eq. (4) worked reasonably well for slowly growing, small-amplitude disturbances. Second, we can place the freestream boundaries at considerable distances above and below the wake centerline. Any adverse effects of using Eq. (4) then will be limited to portions of the flowfield near these boundaries where disturbance levels are small. Near the wake centerline, where most of the disturbance energy is concentrated, the influence of the freestream boundary conditions likely will be negligible.

C. Outflow Boundary ($x = x_o$)

Specification of appropriate outflow boundary conditions presents a significant obstacle to the successful use of DNS for investigations of flows where disturbances exhibit streamwise development. To implement appropriate outflow boundary conditions for our simulations, we make the following observation: Disturbances introduced into the wake at the inflow boundary, as well as any

nonlinearly generated harmonics, require a finite time to travel the length of the computational domain. Therefore, if the duration of the simulation is restricted to less than the transit time of the disturbances, the wake will remain relatively undisturbed at the outflow boundary. Adhering to this restriction on the duration of the simulations, we then can impose Dirichlet conditions at the outflow boundary with the velocity and vorticity set equal to their respective undisturbed values.

However, we note that although these boundary conditions dictate that disturbances cannot be permitted to reach the outflow boundary, in practice one must be more restrictive and require that the outflow boundary and some portion of the computational domain upstream of the outflow boundary remain undisturbed. This restriction limits the influence of the outflow boundary on the disturbances in the wake. However, the size of the domain that must remain disturbance-free cannot be estimated a priori, and instead must be determined by numerical experimentation.

D. Initial Conditions ($t = 0$)

Prior to the imposition of any disturbance forcing, the wake is assumed to be steady and undisturbed. This undisturbed flowfield is obtained by numerically solving the governing equations (1), using the discretization described in Sec. IV. Steady solutions are obtained by integrating the governing equations with respect to time, subject to time-independent boundary conditions, until the maximum residual of the discretized equations falls below 10^{-6} at each grid point in the computational domain (see Sec. IV for a discussion of the grid). Boundary conditions for this calculation are described in detail by Dratler.[8]

IV. Numerical Method

The governing equations (1) are solved numerically using a variant of the method originally developed by Pruett[9] for simulations of spatially developing free shear layers. However, this method has been modified for our work, incorporating improvements in both efficiency and accuracy. For spatial discretization, derivatives are approximated using second-order finite differences. Time integration of the discretized vorticity equations is accomplished using a hybrid alternating direction implicit/Adams–Bashforth scheme of second-order temporal accuracy. The discretized velocity equations are solved using a fast Poisson solver that is based on a method developed by Swarztrauber.[10] Solutions of the discretized vorticity and velocity equations are obtained on a uniform grid composed of N points in the streamwise direction and M points in the cross-stream direction. The overall accuracy of the numerical method is second-order in time and in the streamwise and cross-stream directions. A more detailed description of the numerical method can be found elsewhere.[8,9]

V. Results

In this section, simulations of a monochromatically forced, spatially developing, two-dimensional, flat-plate wake are presented. Numerical solutions were checked by comparing them to linear stability theory and to the experimental measurements of Sato and Kuriki.[1]

A. Comparison with Linear Stability Theory

Comparison of our results to linear stability theory provided a means to check the validity of the numerical solutions for small-amplitude disturbances. For this comparison, we considered an initially undisturbed wake in a computational domain defined by $x_i = 0.3$, $x_o = 0.7$, $y_l = -10$, and $y_u = 10$. The grid was constructed using $N = 1025$ and $M = 257$, which was more than adequate to resolve the fundamental disturbance. For the base-flow calculation, the inflow streamwise velocity profile was

$$u_i(y) = 1 - (1 - U_c)\mathrm{sech}^2(\sigma y/b) \tag{5}$$

with $\sigma = \mathrm{arccosh}(\sqrt{2})$, $U_c = 0.5$, and $b = 1.3$. The wake Reynolds number was $Re = 2 \times 10^5$, with $r = 2.97 \times 10^{-3}$. The forcing parameters were $\beta = 107$, $\alpha_r = 126$, and $A = 0.001$, with the selected forcing frequency somewhat less than the frequency of maximum amplification. The simulation was run for five periods of the fundamental disturbance. Numerical stability dictated the use of 512 time steps for each fundamental disturbance period.

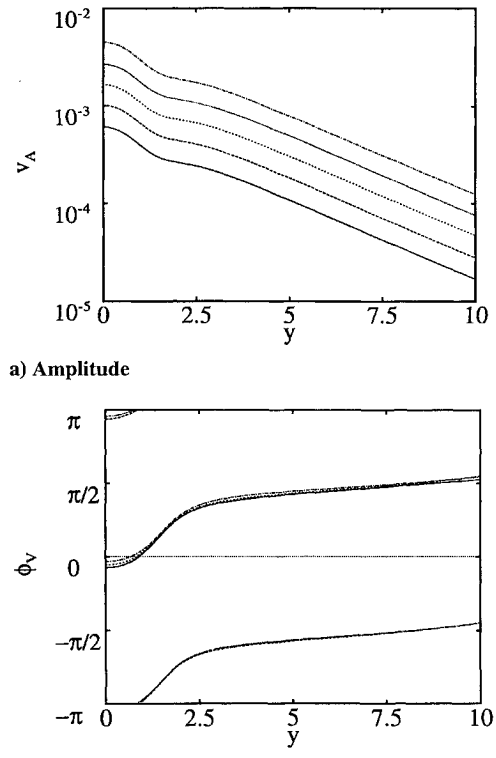

Fig. 2 Amplitude v_A and phase distributions ϕ_v of the fundamental component of the cross-stream velocity: ——, $x = 0.300$; – – –, $x = 0.325$; - - - -, $x = 0.350$; · · · ·, $x = 0.375$; and —·—, $x = 0.400$ and $Re = 2 \times 10^5$. [Distributions at $x = 0.300$ correspond to the cross-stream component of the Orr–Sommerfeld eigenfunction for $\beta = 107$ and were obtained from linear stability analysis of the velocity profile given by Eq. (5). Simulation parameters: $\beta = 107$, $A = 0.001$, $x_i = 0.3$, $x_o = 0.7$, $y_l = -10$, $y_u = 10$, $N = 1025$, and $M = 257$. Amplitude and phase are even about $y = 0$, but are shown for $y > 0$ only.]

Amplitude and phase distributions of the fundamental disturbance are shown in Fig. 2 for several streamwise locations and compared to similar distributions for $x = 0.3$. Recall that $x = 0.3$ is the location of the inflow boundary, so that, as described in Sec. III.A, the amplitude and phase at this location are the amplitude and phase of the Orr–Sommerfeld eigenfunction corresponding to the forcing frequency β. The amplitude distributions (Fig. 2a) show excellent agreement with theory, retaining the shape of the Orr–Sommerfeld eigenfunction through $x = 0.4$, which is approximately two disturbance wavelengths downstream of the inflow boundary. The peak amplitude increases by less than one order of magnitude between $x = 0.3$ and 0.4, indicating a relatively moderate rate of disturbance growth. Phase distributions (Fig. 2b) also show excellent agreement with linear stability theory. The phase distributions are plotted at intervals of $x = 0.025$, which is almost exactly one-half of the fundamental disturbance wavelength. Therefore, the phase difference between consecutive streamwise locations is almost exactly π.

In addition, the amplitude and the phase distributions display the appropriate asymptotic behavior for large $|y|$ that would be expected of small-amplitude disturbances. The amplitude distributions decay exponentially with increasing $|y|$, whereas phases increase linearly with increasing $|y|$. The phases do deviate somewhat from linearity near $y = 10$ because of the assumption of neutral stability implicit in the exponential-decay boundary conditions (4). However, this deviation is quite small and is not observed away from the freestream boundaries.

B. Comparison with Experiment

In this section, calculated disturbance behavior is compared to the measurements of Sato and Kuriki,[1] who conducted an experimental investigation of laminar-turbulent transition in the wake

of a thin plate. These comparisons provide a means to judge the validity of simulations of large-amplitude disturbances. To facilitate comparison, flow conditions were selected to match Sato and Kuriki's[1] experiments as closely as possible. The flow was calculated on a domain defined by $0.03 = x_i \leq x \leq x_o = 0.75$, $-16 = y_l \leq y \leq y_u = 16$ using a grid constructed with $N = 1025$ and $M = 257$. To establish the grid independence of our solutions, simulations were performed for $N = 1025$ with M set to 129, 193, and 257, and for $M = 257$, with N set to 513, 769, and 1025. With this variation in spatial discretization, computed results did not vary significantly.

To match the conditions of Sato and Kuriki's experiments, the wake Reynolds number was set to $Re = 2 \times 10^5$. For this Reynolds number, $r = 2.97 \times 10^{-3}$. For the base-flow calculation, the streamwise velocity at the inflow boundary was taken to be a Gaussian distribution of the form

$$u_i(y) = 1 - (1 - U_c)e^{-a(y/b)^2} \tag{6}$$

with $a = \ell n 2$. In Eq. (6), the parameters $U_c = 0.23$ and $b = 1.15$ were obtained from Goldstein's[11] similarity solution. The selected values of U_c and b are consistent with Sato and Kuriki's[1] experiments.

For the disturbance forcing, the dimensionless frequency was set to $\beta = 172$ (corresponding to 911 Hz), the frequency of maximum streamwise growth (as predicted by linear stability theory) for the inflow velocity distribution [Eq. (6)]. For this frequency, $\alpha_r = 263$. Sato and Kuriki[1] conducted both forced and unforced experiments. For the forced experiments, the wake was excited using a monochromatic acoustic source, with the frequency varied between 480 and 1000 Hz. The frequency of the dominant fluctuation in the unforced case (i.e., the natural frequency) was given as 730 Hz. However, there does appear to be a high degree of uncertainty associated with this value of the natural frequency. On the basis of the data presented in Sato and Kuriki's[1] Fig. 14, which shows the frequency of the dominant wake fluctuation in the absence of forcing, our computations indicate that the natural frequency falls in the range 730–920 Hz. We note that our forcing frequency (911 Hz) lies in this range. In the discussion that follows, our results are compared with measurements from forced and unforced experiments. The experimental amplitude distributions shown in Fig. 3 correspond to a frequency of 730 Hz, the forcing frequency for that experiment. However, the experimental centerline velocity data shown in Fig. 4 are from an unforced experiment, the only data of this type presented by Sato and Kuriki.

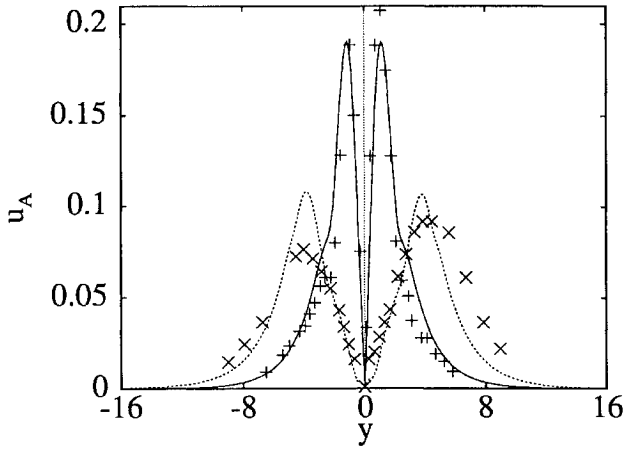

Fig. 3 Amplitude distributions of the fundamental component of the streamwise velocity: ——, numerical simulation, $x = 0.133$; - - - -, numerical simulation, $x = 0.200$; +, Sato and Kuriki,[1] $x = 0.133$; and ×, Sato and Kuriki,[1] $x = 0.200$. [The amplitude data of Sato and Kuriki[1] were plotted in their paper using arbitrary units. The ordinate of these data has therefore been scaled using a linear least-squares technique, with a different scaling used for each streamwise location. Simulation parameters: $Re = 2 \times 10^5$, $\beta = 172$ (911 Hz), $A = 0.001$, $x_i = 0.03$, $x_o = 0.75$, $y_l = -16$, $y_u = 16$, $N = 1025$, and $M = 257$. Experimental forcing frequency 730 Hz.]

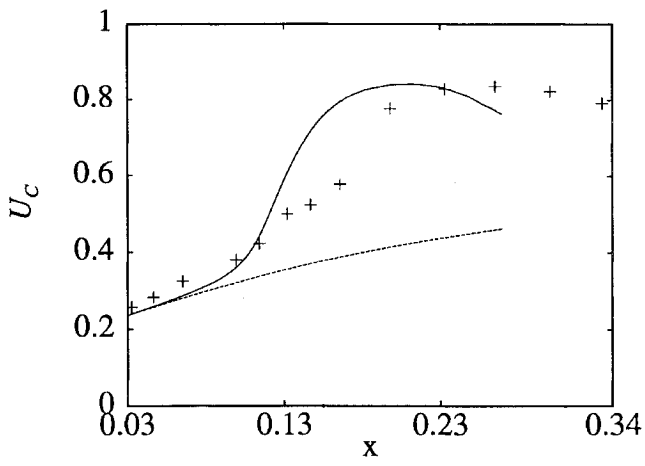

Fig. 4 Centerline velocity U_c vs streamwise distance x: ——, mean-flow value from numerical simulation (forcing frequency 911 Hz); – – –, base-flow value from numerical simulation; and +, mean value from unforced experiments of Sato and Kuriki[1] (simulation parameters: $Re = 2 \times 10^5$, $\beta = 172$, $A = 0.001$, $x_i = 0.03$, $x_o = 0.75$, $y_l = -16$, $y_u = 16$, $N = 1025$, and $M = 257$).

The forcing strength in our simulation was set to $A = 0.001$. It was not possible to determine an appropriate value for A from the data of Sato and Kuriki[1] (for either the forced or the unforced case). However, it was apparent from their results that the disturbance development was governed by linear stability theory for distances downstream of the plate trailing edge of approximately $\bar{x}/\bar{L} \leq 0.10$. Therefore, we set A at a level so that the disturbance development also would be linear for this range of $\bar{x}/\bar{L}$.

The two main discrepancies between our simulation and Sato and Kuriki's[1] experiments are the forcing frequency and the strength. Because both will influence the streamwise location at which nonlinearity becomes important, direct quantitative comparison between simulation and experiment may not be possible. However, we expect qualitative trends to be similar, as discussed below.

The simulation was run for 17 periods of the fundamental disturbance, with numerical stability requirements dictating 128 time steps per period. At the end of the simulation, the disturbed portion of the flowfield had propagated to $x \approx 0.56$, with temporal periodicity attained for $x \lesssim 0.31$, beyond which the temporal behavior is more complicated. The largest streamwise length scale in the time-periodic portion of the wake is the fundamental disturbance wavelength, $\lambda \approx 0.03$. Based on this scale, the disturbed portion of the flowfield is approximately six wavelengths from the outflow boundary. Therefore, the assumption of an undisturbed flowfield at the outflow boundary is satisfied. The influence of the outflow boundary on the numerical solution also was tested by recomputing the solution with $x_o = 1.11$ and $N = 1537$ (i.e., with the same streamwise resolution) but with all other physical and numerical parameters as previously noted. Comparison of the two solutions indicated no observable influence of the outflow boundary.

Figure 3 shows amplitude distributions of the fundamental disturbance for $x = 0.133$ and 0.2, downstream of the location at which the fundamental disturbance saturates. Measured amplitude distributions from Sato and Kuriki[1] are shown for these same locations. The experimental distributions, which Sato and Kuriki[1] plotted in arbitrary units, have been scaled to the numerical distributions using a linear least-squares technique. Because it was not possible to match the forcing level in Sato and Kuriki's experiment, and therefore the comparison shown here is qualitative in nature, a different scaling was used for each streamwise location. This scaling was applied to the ordinate only. For both locations, there is reasonable agreement between the simulated amplitude distributions and the scaled experimental data. We note in particular that between $x = 0.133$ and 0.2 there is a significant redistribution of energy toward the freestream, concomitant with a reduction in peak amplitude. These effects are not predicted by linear stability theory. The reduction in peak experimental amplitude is not an artifact of the scaling. Observed deviations between the simulated and experimental data could be

attributable to the different forcing frequencies (911 Hz in the simulation vs 730 Hz in the experiment), slight differences between the base flows, differences in the level of excitation, or the presence of a broad spectrum of fluctuations in the experiment. Despite these differences, there is good agreement between the simulation and the experiment.

The experimental amplitude distributions shown in Fig. 3 also have been favorably compared to amplitude distributions obtained from temporal direct numerical simulations.[3] This suggests that computed amplitude distributions are not extremely sensitive to variations in methods of computation, forcing parameters, etc. Therefore, we would not expect the level of comparison between our computed distributions and Sato and Kuriki's measurements to be significantly affected by the relatively small differences between our numerical simulation and Sato and Kuriki's experiment.

In Fig. 4, the centerline velocity is shown for the mean and undisturbed flows. Mean centerline velocity from unforced experiments of Sato and Kuriki[1] also is shown. The large increase in centerline velocity implies a significant broadening of the mean flow, and a reduction in its deficit, as compared to the undisturbed flow, and indicates that nonlinear effects are significant. The experimental data in Fig. 4 show similar trends. However, the large velocity increase begins at a different streamwise location in the simulation than in the experiment. We also note that the experimental centerline velocity near $x = 0.03$ is larger than the simulated value. This bias continues downstream until the simulated velocity begins to increase because of nonlinear effects at $x \approx 0.10$, and indicates that the values of U_c and b used to construct the inflow boundary condition for the base-flow calculation [see Eq. (6)] probably were not optimal in terms of producing a base flow representative of Sato and Kuriki's experiment.

The discrepancies between the simulation and experimental data in Fig. 4 likely arise for the same reasons outlined in regard to Fig. 3. However, in contrast to Fig. 3, the experimental data in Fig. 4 are from an unforced experiment. Therefore, an additional cause of the observed discrepancies could be the use of monochromatic forcing in the simulation, which is not representative of the broad spectrum of naturally occurring fluctuations in the experiment. These differences notwithstanding, the numerical and experimental data in Fig. 4 exhibit good qualitative agreement. In addition, simulated mean streamwise velocity distributions (not shown) displayed velocity overshoots as observed by Sato and Kuriki.[1]

C. Additional Discussion of Nonlinear Disturbance Development

To better illustrate nonlinear aspects of the disturbance development, we present results showing the streamwise evolution of the dimensionless disturbance kinetic energy, the fundamental streamwise wave number, and the spanwise vorticity in the large-amplitude regime. The results presented here are from the nonlinear simulation discussed above.

The dimensionless disturbance kinetic energy was calculated using the expression

$$E_l = \frac{1}{2}\int_{y_l}^{y_u} \left[(\hat{U}_l)^2 + r^2(\hat{V}_l)^2\right] \mathrm{d}y \tag{7}$$

In Eq. (7), $l = 0$ corresponds to a zero frequency disturbance (the mean-flow distortion), $l = 1$ corresponds to β (the fundamental disturbance), $l = 2$ corresponds to 2β (the second harmonic), etc. The integral in Eq. (7) is evaluated numerically using Simpson's rule.

The streamwise variation of the disturbance kinetic energy E_l is shown in Fig. 5 for the fundamental disturbance and for three temporal harmonics. In addition, fundamental disturbance kinetic energy growth as obtained from a linear stability analysis of the undisturbed flow is shown. This analysis was performed using a quasiparallel assumption. On the basis of the results shown in Fig. 5, we note that the region of exponential growth of the fundamental disturbance is quite small, being approximately three fundamental wavelengths in extent. The linear region ends when the fundamental disturbance saturates, which is at $x \approx 0.10$. Beyond the point of saturation, the dominant disturbances are the fundamental disturbance ($l = 1$), the mean-flow distortion ($l = 0$), and the second harmonic ($l = 2$).

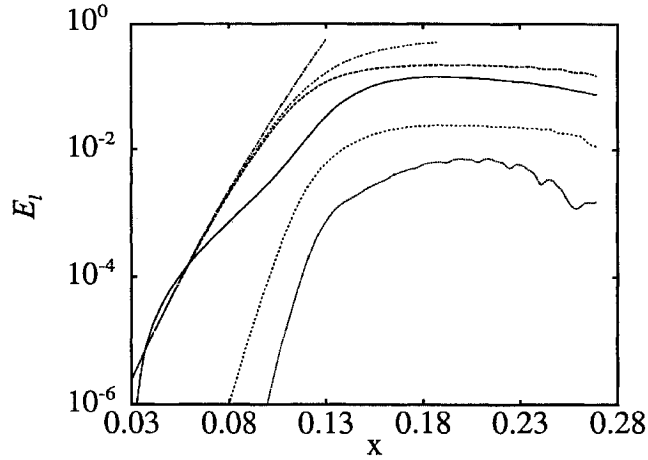

Fig. 5 Disturbance kinetic energy E_l vs streamwise distance x for $Re = 2 \times 10^5$: ——, $l = 0$; – – –, $l = 1$; - - - -, $l = 2$; · · · ·, $l = 3$; —·—, Orr–Sommerfeld stability analysis of the undisturbed flow; and - - - - -, Orr–Sommerfeld stability analysis of the mean flow (simulation parameters: $\beta = 172, A = 0.001, x_i = 0.03, x_o = 0.75, y_l = -16, y_u = 16, N = 1025$, and $M = 257$).

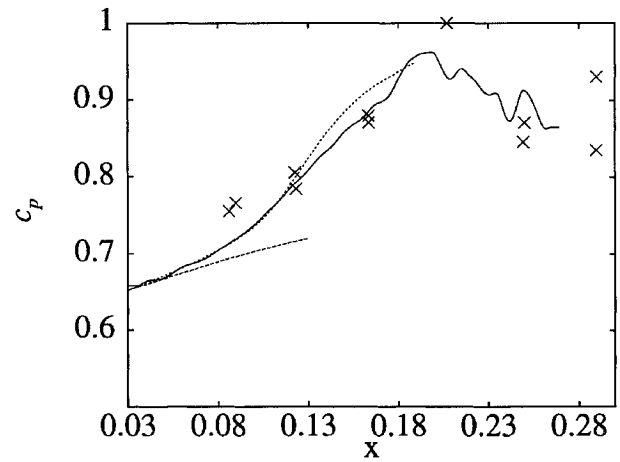

Fig. 6 Phase speed c_p of the fundamental disturbance vs streamwise distance x: ——, numerical simulation (forcing frequency 911 Hz); – – –, Orr–Sommerfeld stability analysis of the undisturbed flow; - - - -, Orr–Sommerfeld stability analysis of the mean flow; and ×, forced transition experiments of Sato and Kuriki[1] (forcing frequency 730 Hz) (simulation parameters: $Re = 2 \times 10^5, \beta = 172, A = 0.001, x_i = 0.03, x_o = 0.75, y_l = -16, y_u = 16, N = 1025$, and $M = 257$).

These three disturbances contain approximately 95% of the total disturbance kinetic energy. The mean-flow distortion and second harmonic are dominant near the wake centerline, whereas the fundamental is dominant away from the centerline. This is consistent with Sato and Kuriki's[1] measurements.

Saturation, which occurs at $x \approx 0.10$, coincides with the large increase in mean centerline velocity seen in Fig. 4. Increases in mean centerline velocity, which tend to decrease the mean shear, are known to have a stabilizing influence on small-amplitude disturbances and may have a similar effect on large-amplitude disturbances. To quantify this effect, we performed a linear stability analysis (Orr–Sommerfeld) of the mean flow, i.e., the base flow plus the mean-flow distortion. The streamwise variation of kinetic energy predicted by this analysis (Fig. 5) clearly shows saturation of the fundamental disturbance amplitude, although the absolute kinetic energy level is overpredicted. This suggests that fundamental disturbance saturation may simply be attributable to the stabilization (in a linear sense) of the mean flow resulting from nonlinear interactions. This simple view of saturation is supported by the results of Ko et al.,[12] who employed integral methods to investigate nonlinear disturbance development in wakes. For mixing layers, a similar saturation mechanism has been proposed.[13]

In Fig. 6, the streamwise variation of fundamental disturbance phase speed is shown. The increase in phase speed that occurs for

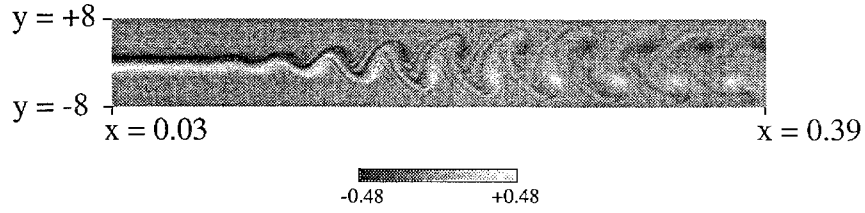

Fig. 7 Spanwise vorticity ω_z in the xy plane: $Re = 2 \times 10^5$; $t = 0.62$; $0.03 \le x \le 0.39$; $-8 \le y \le 8$. Flow is from left to right. Simulation parameters: $\beta = 172, A = 0.001, x_i = 0.03, x_o = 0.75, y_l = -16, y_u = 16, N = 1025$, and $M = 257$.

$x \geq 0.08$ is reasonably well predicted by the mean-flow stability analysis, providing additional evidence to support our contention that initial nonlinear evolution of the fundamental disturbance may be governed by the linear stability of the mean flow. In contrast, stability analysis of the undisturbed base flow predicts a more gradual increase in phase speed. In addition, the fundamental phase speed from the simulation exhibits reasonable agreement with the measurements of Sato and Kuriki.[1]

Instantaneous spanwise vorticity is shown in Fig. 7 for $t = 0.62$ (17 fluctuation periods). The most prominent feature of the vorticity field is the vortex street that forms for $x > 0.21$. As the vortex street develops, positive vorticity (white and light gray areas), which near the inflow boundary is confined to $y < 0$, is convected upward across the wake centerline. At the same time, negative vorticity (black and dark gray areas) from $y > 0$ is convected downward across the wake centerline. If we neglect viscous diffusion, then

$$\frac{D\omega_z}{Dt} = 0 \tag{8}$$

and the spanwise vorticity associated with a particular fluid element is invariant with time. Therefore, the positive vorticity observed for $y > 0$ is associated with fluid that originated below the wake centerline and was convected upward as a result of the disturbance flowfield. Likewise, the negative spanwise vorticity below the centerline is associated with fluid originating above. This indicates a high degree of cross-stream convection and mixing. For $x > 0.25$, the spanwise vorticity convected across the wake centerline coalesces into small vortices positioned adjacent to oppositely signed Kármán vortices. These small vortices appear to be similar to the secondary vortices observed by Zabusky and Deem[3] in their simulations of temporally evolving wakes.

D. Influence of Forcing Strength on Disturbance Behavior

In Sec. V.C it was shown that exponential growth of the fundamental disturbance led to saturation downstream of the inflow boundary. This saturation distance clearly will vary with forcing strength. Stronger forcing (i.e., stronger than $A = 0.001$ used in Sec. V.C) should lead to saturation farther upstream whereas weaker forcing should have the opposite effect. In addition, other aspects of disturbance behavior might depend on forcing strength. To assess the effects of forcing strength on disturbance behavior, we reran the simulation discussed in Sec. V.C with $A = 0.01$, with all other physical and numerical parameters as discussed in Secs. V.B and V.C. We note that $A = 0.01$ is less than the excitation level that would result in fundamental disturbance saturation at the inflow boundary.

In Fig. 8, we show the evolution of disturbance kinetic energy for $A = 0.001$ (for which results were described in detail in Secs. V.B and V.C) and $A = 0.01$. For the fundamental disturbance, exponential growth at small x is observed for both $A = 0.01$ and $A = 0.001$. For $A = 0.01$, the fundamental disturbance saturates farther upstream, as expected for stronger forcing. However, we note that the maximum kinetic energy levels for both forcing strengths are similar (in the range $E_1 \approx 0.22$–0.25). In addition, although there are obvious quantitative differences, the kinetic energy curves for $A = 0.01$ and $A = 0.001$ are remarkably similar in character. Both show regions of exponential growth followed by a saturated state in which fundamental disturbance energy varies relatively little.

The second harmonic, as characterized by disturbance kinetic energy, also exhibits trends that differ little with forcing strength. For both forcing strengths, the second harmonic exhibits strong growth at small x and more gradual variation at larger x, as was the case for the fundamental disturbance. However, for the stronger forcing, the second harmonic achieves its maximum energy level farther upstream.

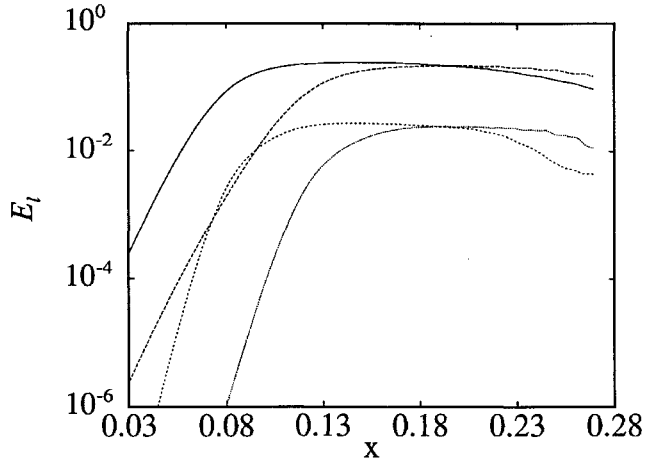

Fig. 8 Disturbance kinetic energy E_l vs streamwise distance x for $Re = 2 \times 10^5$: ——, $A = 0.01, l = 1$; – – –, $A = 0.001, l = 1$; - - - -, $A = 0.01, l = 2$; and · · · ·, $A = 0.001, l = 2$ (other simulation parameters: $\beta = 172, x_i = 0.03, x_o = 0.75, y_l = -16, y_u = 16, N = 1025$, and $M = 257$).

These results suggest an insensitivity of saturated amplitude to variations in forcing strength. Similar behavior has been observed in experiments of axisymmetric mixing layers[14] and numerical simulations of plane mixing layers.[13]

VI. Conclusions

Direct numerical simulations were employed to investigate the spatial evolution of a monochromatically forced, incompressible, low-speed wake behind a thin flat plate aligned parallel to a uniform freestream. The results of these simulations, which were restricted to two dimensions, demonstrated good overall agreement with experimental measurements of Sato and Kuriki.[1] Areas of agreement include the presence of a region governed by linear stability theory (for sufficiently weak forcing) in which growth rates are quite large, a nonlinear region in which fluctuation amplitudes vary more gradually with streamwise distance than in the linear region, the formation of significant second-harmonic and mean-flow distortion components, and the development of a Kármán vortex street at large two-dimensional disturbance levels. The good agreement between the two-dimensional simulations and Sato and Kuriki's experiment (for which low-level three-dimensional fluctuations were present) suggests that the neglect of three-dimensionality is justified for simulations of the early linear and nonlinear stages of transition in wakes behind thin plates.

Our results also indicate that fundamental disturbance saturation can be predicted, at least qualitatively, from a linear stability analysis of the distorted mean flow. This suggests a simple model for saturation in which nonlinear self-interactions of the fundamental disturbance distort the mean flow, while the enhanced linear stability of this distorted flow reduces the fundamental disturbance growth rate to cause saturation. This simple view of saturation is supported by the results of others.

The vortex street shown in Fig. 7 is clearly a large-amplitude phenomenon, with its formation occurring downstream of the onset of

fundamental disturbance saturation. The vortex street is accompanied by formation of secondary vortices whose development appears to be driven by strong cross-stream convection in the vortex-street. Similar vortex-street development has been observed experimentally.

Our two-dimensional simulations also indicate that variations in forcing strength do not substantially alter the disturbance behavior. The main effect of stronger forcing is to move the onset of nonlinearity, and hence saturation, farther upstream. In addition, the kinetic energy level of disturbances in the saturated state appears to be relatively insensitive to forcing strength, suggesting that nonlinear disturbance development is quantitatively, but not qualitatively, influenced by this parameter, provided that the initial disturbance development is linear. This suggests that in this flow, the forcing strength in a simulation or experiment can be set to a value giving a convenient range of linear disturbance development.

Acknowledgments

Financial support for this work was provided by the NASA Graduate Student Researchers Program (NASA Grant NGT-50074) and the U.S. Air Force Office of Scientific Research (AFOSR Grant 85-0146). The first author was supported by the University of Illinois during final preparation of the manuscript. Computer resources were provided by the National Aerodynamics Simulation Facility and the San Diego Supercomputer Center. Finally, the authors wish to thank A. J. Pearlstein for his helpful review of the manuscript.

References

[1]Sato, H., and Kuriki, K., "The Mechanism of Transition in the Wake of a Thin Flat Plate Placed Parallel to a Uniform Flow," *Journal of Fluid Mechanics*, Vol. 11, No. 3, 1961, pp. 321–352.

[2]Heinemann, H. J., Lawaczeck, O., and Bütefisch, K. A., "Von Kármán Vortices and Their Frequency Determination in the Wakes of Profiles in the Sub- and Transonic Regimes," *Symposium Transsonicum II*, Springer–Verlag, New York, 1976, pp. 75–82.

[3]Zabusky, N. J., and Deem, G. S., "Dynamical Evolution of Two-Dimensional Unstable Shear Flows," *Journal of Fluid Mechanics*, Vol. 47, No. 2, 1971, pp. 353–379.

[4]Hannemann, K., and Oertel, H., "Numerical Simulation of the Absolutely and Convectively Unstable Wake," *Journal of Fluid Mechanics*, Vol. 199, Feb. 1989, pp. 55–88.

[5]Maekawa, H., Mansour, N. N., and Buell, J. C., "Instability Mode Interactions in a Spatially Developing Plane Wake," *Journal of Fluid Mechanics*, Vol. 235, Feb. 1992, pp. 223–254.

[6]Huerre, P., and Monkewitz, P. A., "Absolute and Convective Instabilities in Free Shear Layers," *Journal of Fluid Mechanics*, Vol. 159, Oct. 1985, pp. 151–168.

[7]Fasel, H., "Investigation of the Stability of Boundary Layers by a Finite-Difference Model of the Navier–Stokes Equations," *Journal of Fluid Mechanics*, Vol. 78, No. 2, 1976, pp. 355–383.

[8]Dratler, D. I., "Numerical Investigation of Laminar-Turbulent Transition in a Flat Plate Wake," Ph.D. Dissertation, Dept. of Aerospace and Mechanical Engineering, Univ. of Arizona, Tucson, AZ, 1990.

[9]Pruett, C. D., "Numerical Simulation of Nonlinear Waves in Free Shear Layers," Ph.D. Dissertation, Dept. of Mathematics, Univ. of Arizona, Tucson, AZ, 1986.

[10]Swarztrauber, P. N., "Methods of Cyclic Reduction, Fourier Analysis and the FACR Algorithm for the Discrete Solution of Poisson's Equation on a Rectangle," *SIAM Review*, Vol. 19, No. 3, 1977, pp. 490–501.

[11]Goldstein, S., "Concerning Some Solutions of the Boundary Layer Equations in Hydrodynamics," *Proceedings of the Cambridge Philosophical Society*, Vol. 26, No. 1, 1930, pp. 1–30.

[12]Ko, D. R., Kubota, T., and Lees, L., "Finite Disturbance Effect on the Stability of a Laminar Incompressible Wake Behind a Flat Plate," *Journal of Fluid Mechanics*, Vol. 40, No. 2, 1970, pp. 315–341.

[13]Metcalfe, R. W., Orszag, S. A., Brachet, M. E., Menon, S., and Riley, J. J., "Secondary Instability of a Temporally Growing Mixing Layer," *Journal of Fluid Mechanics*, Vol. 184, Nov. 1987, pp. 207–243.

[14]Freymuth, P., "On Transition in a Separated Laminar Boundary Layer," *Journal of Fluid Mechanics*, Vol. 25, No. 4, 1966, pp. 683–704.